RSC Advances

ROYAL SOCIETY OF CHEMISTRY

www.rsc.org/advances

Journal Name

ARTICLE

Bendable Graphene/Conducting Polymers Hybrid Films for Freestanding Electrodes with High Volumetric Capacitances

Received 00th January 20xx,
Accepted 00th January 20xx

DOI: 10.1039/x0xx00000x

www.rsc.org/

Lu Mao[#], Meng Li[#], Junmin Xue and John Wang*

Bendable freestanding films composed of reduced graphene oxide (RGO) and one dimensional conducting polymers (CPs) including polyaniline (PANI) and polypyrrole (PPy) are successfully fabricated by self-assembly assisted filtration method. The morphology and intrinsic properties of both components are well preserved and the desired synergetic effects are achieved. The intercalated one dimensional CPs act as not only pseudocapacitors to improve the overall capacitance but also effective framework to open the penetrative channels for electrolyte. The hybrid freestanding electrodes thus obtained exhibit superior performance in terms of gravimetric capacitance, volumetric capacitance and cycling stability. For example, at the current density of 0.2 A g^{-1}, RGO/PPy film electrode gives rise to a gravimetric capacitance of 374 F g^{-1} and volumetric capacitance of 355 F cm^{-3}; while RGO/PANI film electrode yields a high gravimetric capacitance of 540 F g^{-1} and volumetric capacitance of 616 F cm^{-3}. Both RGO/PANI and RGO/PPy hybrid film electrodes deliver good cycling stabilities with ~86% of original capacitances being retained after 5000 cycles.

Introduction

Over the past decade, there have been continuing demands for the development of sustainable and renewable energy devices due to the growing global energy use along with the diminishing supply of fossil fuels and environmental problems. Among them, supercapacitors as energy storage devices are of huge technological interest recently due to their high power density, long cycle life, and rapid charging-discharging rate.[1-3] Based on the energy storage mechanisms, supercapacitors are divided into two categories: electrical double layer capacitor (EDLC) mainly based on porous carbon materials and pesudocapacitor based on conducting polymers and metal oxides/hydroxides. Indeed, supercapacitors have been widely used in many critically important technical areas, such as electrical and hybrid vehicles, power grids, and aerospace applications.[4] With the growing demand for portable and wearable electronic devices, flexible energy storage devices are gaining more and more attentions.[5-7] In the fabrication of such flexible supercapacitors/batteries, freestanding binder-free electrodes with a rationally designed structure and optimal composite composition play a large part in the capacitive performance of the device.[5] Graphene, a well-developed two-dimensional carbon material, with numerous advanced properties such as high electrical conductivity (106 S cm^{-1}), excellent mechanical flexibility, high tunable specific surface area (calculated theoretical value of ~2630 m^2 g^{-1}) and chemical stability, is regarded as one of the most suitable candidates to realize such bendable freestanding film electrodes.[8-12] Recent success in solution phase synthesis of graphene from graphite in large quantity through chemical conversion of graphene oxide further arouses interest in the use of graphene as building blocks to construct cost-effective and structurally defined macroscopic materials.[13-15] In particular, chemically reduced graphene oxide (RGO), which is similar to graphene in a number of aspects, is able to form stable colloids without any surfactants and realize the assembly of RGO sheets into freestanding film ultimately.[16] However, during the fabrication process, freestanding films composed of RGO nano-sheets are readily to be aggregated due to the strong van der Waals attraction, which leads to the increased difficulty of ions diffusion as well as slow electron transport rate and therefore unsatisfactory capacitive performance. Hence, various nanostructured functional materials, such as metal oxides,[17] carbon nanotubes,[18] and conducting polymers,[19, 20] have been hybridized with graphene

[a] Department of Materials Science and Engineering, National University of Singapore, Singapore, 117573. E-mail: msewangj@nus.edu.sg (Prof. J. Wang)
[#] Lu Mao and Meng Li contributed equally to this work.
Electronic Supplementary Information (ESI) available: [SEM images of PPy and PANI, additional TEM images, XRD pattern of the RGO film and cycling performance of pure PANI and PPy]. See DOI: 10.1039/x0xx00000x

in pursuing improved capacitive performance. Conducting polymers (CPs) have attracted considerable attention as promising electrode materials for high performance supercapacitors owing to their unusual electronic properties. In addition to a relatively high conductivity in oxidized and doped states, simple CPs, such as polypyrrole, polyaniline, and polythiophene can deliver high specific capacitances via pseudocapacitive charge storage mechanism, originating from a fast and reversible p-doping (oxidation) and n-doping (reduction) of the conjugated double bonds in polymer networks.[2] Furthermore, conducting polymers with one-dimensional nanostructures exhibit superior electrochemical properties compared to three-dimensional structures due to their smaller dimensions and high aspect ratios.[21]

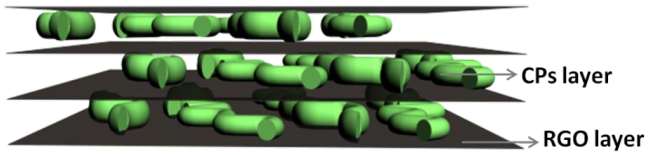

Figure 1: Schematic illustrating the intercalated structure of RGO/CPs hybrid film.

Herein, we present a study on the fabrication of bendable film electrodes with optimized nanocomposite structure based on the interpenetrative nanocomposites of graphene and conducting polymers. In such purposely designed structure, as illustrated in Figure 1, graphene sheets are densely packed, conducting polymers are intercalated in between the densely stacked graphene, and these 1D CPs are uniformly distributed in the carbon matrix. The key of this design to enable synergistic effects from the both components. Graphene serves as a high-surface-area substrate for the decoration of 1D conducting polymer to provide efficient electronic transportation. The 1D conducting polymers act not only as effective space inhibitor to prevent the aggregation of graphene but also pseudocapacitor to improve the overall capacitance. In addition to graphene nanosheets, which keep the integrity of the film and offer flexibility, CPs are essential for the formation of a flexible film to provide mechanical reinforcement under the hydrogen bond and $\pi - \pi$ stacking with graphene layers.[22, 23] The morphology and intrinsic properties of the two components are well preserved in order to achieve a better synergetic effect. The freestanding film electrodes thus obtained are expected to deliver superior performance in terms of capacitance (both volumetric and gravimetric performance) and rate capability.

Experimental

Material synthesis

Synthesis of aqueous dispersions of reduced graphene oxide (RGO) sheets

Graphene oxide (GO) dispersion (5 g L^{-1}) was purchased from Graphene Laboratories Inc. Graphene oxide suspension was then dispersed in water to create 1 mg mL^{-1} dispersion followed by ultrasonication for 30 min. In a typical preparation procedure, the resulting homogeneous dispersion (50 mL, 1 mg mL^{-1}) was mixed with 0.3 mL of hydrazine solution (35 wt% in water, Aldrich) and 0.42 mL of ammonia solution (28 wt% in water, Aldrich) in 100 ml round bottom flask. Reduction was observed in about 30 min when the brown color GO suspension became black. The suspension was allowed to stir at room temperature for one day. Excess hydrazine in the resulting dispersions was removed by dialysis against a 0.5% ammonia solution once the reduction is complete.[24]

Synthesis of 1D conducting polymers (CPs)

PANI nanofibers were synthesized by a rapid mixing reaction. Aniline was first distilled under vacuum to remove the oxidation impurities. The purified aniline was dissolved in 1 M HCl aqueous solution at a concentration of 0.3 M. While maintaining vigorous stirring at room temperature, an equal volume of 0.08 M ammonium peroxydisulfate in 1 M HCl aqueous solution was rapidly poured into the aniline solution. Polymerization was observed in about 5 min when the characteristic green colour of polyaniline emeraldine salt appeared. The mixture was allowed to stir at room temperature overnight. The solid PANI was collected by vacuum filtration and repetitively washed with water and ethanol until the filtrate became colourless. After having been dried under vacuum at 80 ^{o}C, the deep green PANI nanofibers were dispersed in water to create 1 mg mL^{-1} dispersion followed by sonication for 1 h to form homogeneous dispersion.[25]

PPy nanowires were prepared through a simple strategy using lamellar inorganic/organic mesostructures as templates. Typically, 0.3 mmol cetyltrimethylammonium bromide (CTAB) was dissolved in 30 mL of distilled water to form a homogeneous solution. 60 µL of pyrrole monomer was added to the above surfactant aqueous solution. The mixture was then vigorously stirred for 10 min and subsequently cooled to 0–5 ^{o}C. Pre-cooled ammonium persulfate (APS) aqueous solution (0.90 mmol, 6.5 mL) was added dropwise into the mixture with simultaneous vigorous stirring. The solution was allowed to stand at 0–5 ^{o}C for a further 24 h. The solid PPy was collected by vacuum filtration, washed with D.I. water and ethanol, and dried in a vacuum oven under vacuum at 80 ^{o}C. The black PPy sample was then dispersed in water to create 1 mg mL^{-1} dispersion followed by sonication for 1 h to form homogeneous dispersion.[26]

Preparation of RGO/CPs Film

PANI sample and PPy sample were respectively dispersed in water to create 1 mg mL^{-1} dispersion followed by sonication for 1 h to form homogeneous dispersions, respectively. The suspensions of the as-prepared RGO and conducting polymers were mixed via ultrasonication followed by vacuum filtration through a mixed cellulose ester filter membrane (200 nm pore size) to obtain hybrid films with intercalated structure. The weight feed ratio of RGO to CPs was varied as 7:3 and 5:5 and the resulting hybrid films were named as RGO/PANI(30%) Film, RGO/PANI(50%) Film, RGO/PPy(30%) Film, and RGO/PPy(50%) Film, respectively. Typically, the reduced graphene oxide dispersion thus obtained (17.5 mL) was mixed with PANI water

dispersion (7.5 mL) and sonicated for one hour to form homogenous suspension. The suspension was then vacuum filtered through a mixed cellulose ester filter membrane (200 nm pore size). It is recommended to use the miniwatt vacuum pump with relative less suction in order to provide enough self-assembly duration. After finishing the filtration process, the

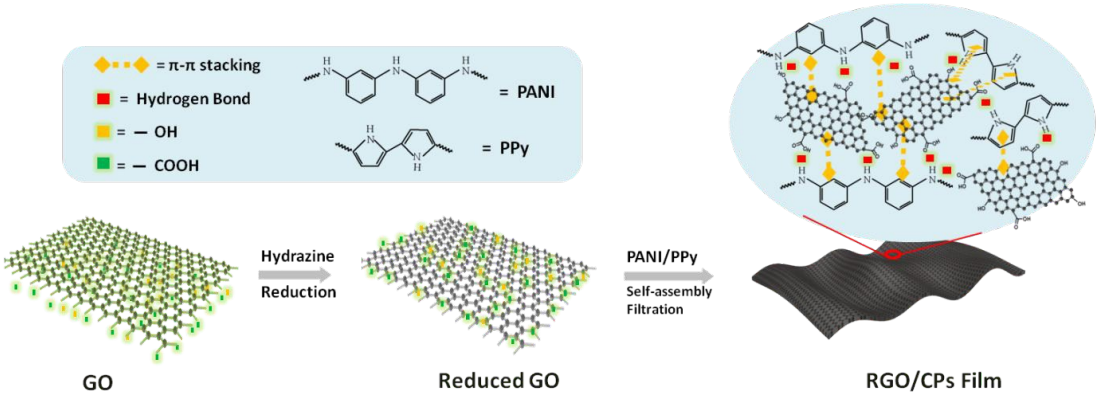

Figure 2: Schematic of the process for preparation of RGO/CPs hybrid film and the chemical interactions within.

hybrid film was kept on the filter membrane for a few hours before carefully peeling off. The graphene paper was cut by a razor blade into rectangular pieces of 1 cm × 1 cm for electrochemical testing.

Material characterization

The morphology and structure of each sample were studied using scanning electron microscopy (SEM) (XL30 FEG-SEM Philips) and transmission electron microscopy (TEM) (JEM2010F). The notch cross-section was prepared by focused ion beam milling using an AURIGA 60 FIB-SEM Crossbeam (ZEISS, Germany). Prior to milling, the top surface of the material was protected with ~100 nm layer of Pt metal induced by e-beam assisted gas deposition, followed by ~400 nm layer of Pt induced by ion-beam assisted gas deposition. Using a 30 kV; 4 nA focused ion beam (FIB) current a coarse incision was milled directly into the surface of the material in order to achieve a viewing channel for the SEM imaging. The notch of about 5 µm in width was fine-polished using a 30 kV: 50 pA FIB probe current. The cross-section face was imaged using the 30 µm aperture at 1kV accelerating voltage, and the In-lens secondary electron and energy-selective backscatter detectors. X-ray powder diffraction (XRD) patterns were collected on a Bruker AXS X-ray powder diffractometer (D8 Advance, Cu Kα, λ = 0.154060 nm). The surface function groups in the hydrogel nanocomposite were investigated using X-ray photoelectron spectroscopy (XPS) (AXIS Ultra). Raman spectra were acquired on a Renishaw inVia Raman microscope using a 514 nm laser under ambient conditions. Conductivity measurements were carried out on a Signatone S-301-6 Conductivity Meter using four-point probe head. The electrochemical performance of the graphene/conducting polymer/CNTs film electrode was characterized by three-electrode system comprising with free standing film directly as the working electrode (~1 cm^2 area; material mass: ~1 mg), Ag/AgCl as reference electrode and platinum (Pt) as counter electrode in a 1 M H_2SO_4 aqueous electrolyte.

Results and discussion

A schematic illustration for preparation of RGO/CPs hybrid film is presented in Figure 2. GO is largely reduced to RGO by hydrazine first, while some of the oxygen-containing functional groups, such as –OH and –COOH groups, still remain on the edge of RGO. Since RGO is able to readily disperse into single or few layers in aqueous solution under sonication, it is beneficial for the adsorption of PANI or PPy to the surface of RGO sheets under stirring. As PANI or PPy dispersions are added into the RGO suspension, these CPs are absorbed onto the surfaces/edge of RGO sheets due to the strong π – π stacking between backbones of CPs and graphene basal planes, as well as the hydrogen bond within functional groups.[27] Besides, the residual carboxylic groups at the edges of RGO can also lead to the electrostatic interaction with PANI/PPy.[28] All of these interactions help make the CPs homogeneously coat onto the RGO nanosheets.

Journal Name

ARTICLE

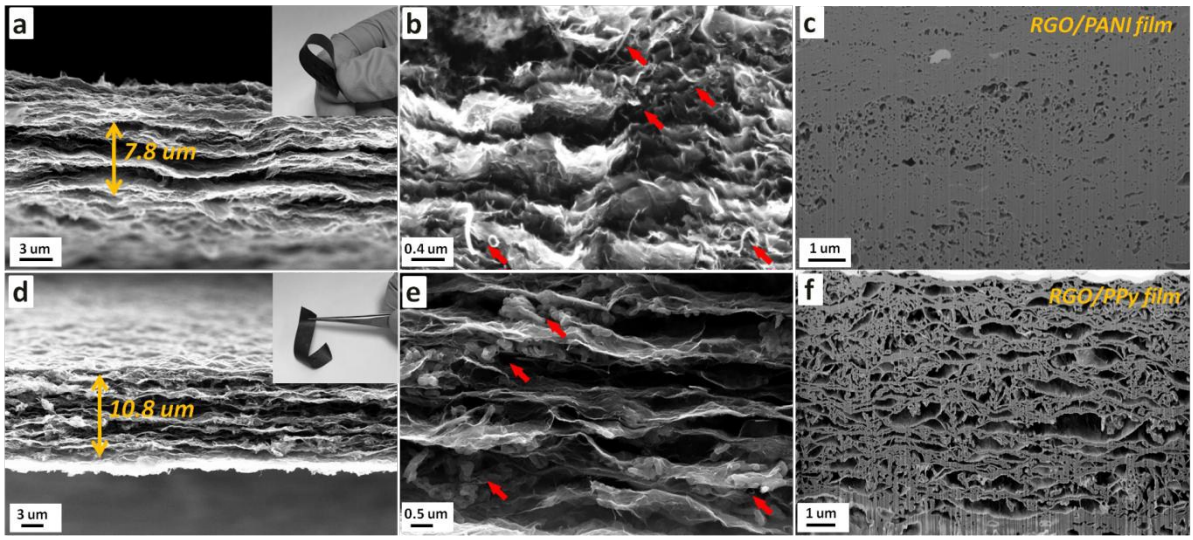

Figure 3: Morphology characterizations of the hybrid films. Cross sectional SEM images of RGO/PANI(30%) film (a,b) and RGO/PPy(30%) film (d,e) at different magnifications, PANI and PPy indicated by red arrows, inset optical images show the flexibility of films; Side view of the focused-ion beam (FIB) etched films in parallel direction to graphene sheets (c) and (f).

The morphology and structure characterizations of the hybrid films are presented in Figure 3. The pure 1D PANI shows uniform fibrous structures with hundreds of nanometers in length and about 50 nm in width, while pure 1D PPy exhibits uniform nanowire morphology with diameters around 200 nm and lengths up to several micrometers, as shown in Figure S1. The lower magnified SEM images in Figure 3a and 3d indicate the thickness of the RGO/PANI film RGO/PPy film thus obtained are around 7.8 and 10.8 µm, respectively. The inset photographs show their excellent flexibility. The cross sectional SEM images (Figure 3b and 3e) in higher magnification show a uniform intercalation of 1D conducting polymers into the dense graphene layers. In addition, the closely stacked graphene sheets become much more porous in the presence of 1D conducting polymers. The TEM images in Figure S2 reveal that both components are well linked, and such linkage is quite critical for the formation of a flexible film.[29] In order to further observe the inner structure of the films, the ion beam milling was performed with the notch drilled in the films (Figure 3c and 3f). The cross sectional SEM images of the notch in Figure 3c&f show the uniform distribution of PANI/PPy among graphene layers. In particular, numerous punctuate pores in RGO/PANI film (Figure 3c) and slit-like pores in RGO/PPy film (Figure 3f) derived from the homogeneously dispersed polymer fibers can provide a huge accumulation place for electrolyte ions and allow for a high capacity of energy storage. These advantages will ultimately result in a remarkably enhanced energy storage performance.

The XRD patterns of PANI, PPy and hybrid films are shown in Figure 4. The pure PANI sample in Figure 4a exhibits several broad reflection peaks with the most intense peak at 2θ = 25.4°, indicating some crystalline order in the bulk PANI samples.[30] The hybrid film of RGO/PANI not only exhibit peaks from PANI at 2θ = 25.4° but also broad diffraction peaks from RGO around 24.8° and 42.8° (Figure S3 for the XRD pattern of pristine RGO film), attributing to the graphite-like structure (0 0 2) and (1 0 0), respectively. RGO/PANI film exhibits reflection peaks at 23.8°, corresponding to an interlayer distance of ~0.37 nm. The broad peak of carbon somewhat overlaps with the peaks of PANI at 2θ = 20.5°. In Figure 4b, pure PPy sample exhibits a weak and broad band at about 2θ = 26° (i.e., d = 0.34 nm), indicating its amorphous nature. For the XRD pattern of RGO/PPy films, the weak broad peak of PPy somewhat overlaps with peaks from RGO at around 23 and 43°. RGO/PPy film exhibit (0 0 1) reflection peaks at 24°, corresponding to an interlayer distance of 0.37 nm. The XRD data of hybrid films reveal that RGO and CPs are well mixed without any crystalline structural changes. The broad peak observed also indicates that the graphene sheets are loosely stacked in the hybrid films. The (0 0 1) reflection peaks of hybrid films shift to a lower degree compared with RGO film indicating the increased

interlayer distance due to the intercalation of CP into graphene layers.

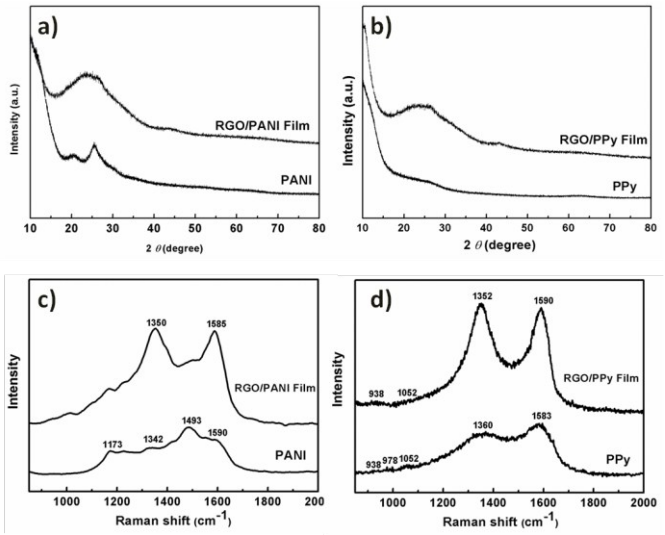

Figure 4: X-ray diffraction patterns (a, b) and Raman spectra (c, d) of RGO/CPs films.

The development of RGO/PANI hybrids was also confirmed by Raman scattering (Figure 4c). For pristine PANI sample, the C–H bending of quinoid ring at 1173 cm^{-1}, C–N^{+} stretching at 1342 cm^{-1}, N=C=N stretching vibration of the quinoid di-imine units at 1493 cm^{-1}, and C–C stretching deformations in benzoid ring at 1590 cm^{-1} are obviously observed.[30, 31] RGO generally displays characteristic D and G bands at around 1350 and 1585 cm^{-1}, respectively, corresponding to the well-documented D mode of a sp2-hybridized carbon and the G mode related to the vibration of a sp3, hybridized carbon, respectively.[15, 23] The typical D-band, G-band and the characteristic bands of PANI are also be observed in the spectrum of RGO/PANI film. In Figure 4d, PPy exhibits the characteristic bands at 1583 and 1360 cm^{-1} due to stretching of the π conjugated structure and the ring stretching mode of PPy, respectively.[32, 33] The peak located at 1052 cm^{-1} corresponds to the C–H in-plane deformation. The bands at about 978 and 938 cm^{-1} are attributed to ring deformations in association with the dication (bipolaron) and the radical cation (polaron), respectively.[23] The Raman spectrum of RGO/PPy hybrid film (Figure 4d) shows bands which are related to the RGO and PPy components. Two peaks at 1590 and 1352 cm^{-1} are identical to the bands of RGO and peaks at 938 and 1052 cm^{-1} belong to pure PPy.

Information about the chemical compositions of the hybrid films is further confirmed by X-ray photoelectron spectroscopy (XPS) as shown in Figure 5. Hybrid films mainly show C 1s, N 1s and O 1s peaks at 284.6, 399.7 and 532.4 eV, as seen in the survey spectra of Figure 5a. The presence of N 1s indicates that both CPs of PANI and PPy are deposited onto the graphene surface. The C1s of XPS spectrum (Figure 5b) can be deconvoluted into peaks at 284.6, 285.8, 286.7 and 288.2 eV, attributed to the typical signals of C-C, C–N band, C–O (hydroxyl and epoxy groups) and C=O (carboxyl groups), respectively.[34, 35] The evolution of N 1s is not shown here since the signal is not high. The relative intensities of oxygen functionalities in this spectrum are much weaker than those of GO (Figure 5d), demonstrating a high degree of deoxygenating and successful reduction of GO to RGO during the chemical reduction process,

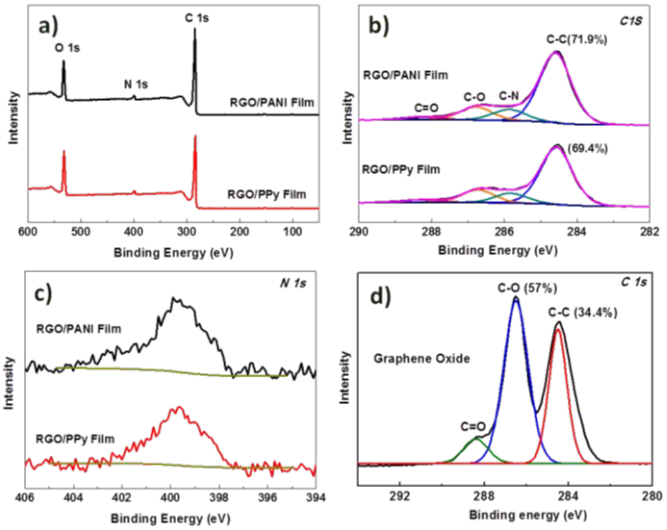

Figure 5: XPS survey spectra (a), C 1s spectra (b), N 1s spectra (c) of RGO/CPs hybrid films; C 1s spectra of graphene oxide (d).

which effectively increases the electrical conductivity of graphene based film.

Figure 6a and 6b show the cyclic voltammograms of the hybrid film electrodes with a potential window from -0.2 to 0.8 V (vs Ag/AgCl) at a scan rate of 5 mV s^{-1}. Two couples of redox peaks are also observed from the CV curves in Figure 6a, which are attributed to the leucoemeraldine/emeraldine and emeraldine/pernigraniline transitions of PANI. Furthermore, the CV curves in Figure 6b are nearly rectangular in shape with slight redox peaks at 0 and 0.5 V, indicating good charge propagation and ion response within the electrode. As can be seen in all the CV curves of these four samples, the features for PANI and PPy in their CV results increase with the increasing PANI and PPy weight percentage in the hybrid films. The hybrid film electrodes were further examined by the electrochemical impedance spectroscopic (EIS) analysis in the frequency range of 0.1–10 kHz, and results of which are shown in Figure 6c and 6d. Equivalent series resistances of all materials are around 0.5 Ω, which can be determined from the x intercept of the Nyquist plots, implying the good conductivity of the hybrid films and electrolyte. All the plots exhibit semicircles over the high frequency region, which is typical for supercapacitors with obvious pseudo-behavior, indicating the interfacial charge-transfer resistance of the material. Smaller semicircles and shorter Warburg region of RGO/PANI(30%) film and RGO/PPy PANI(30%) film compared with RGO/PANI(50%) film and RGO/PPy(50%) film can be found on the plots, suggesting their smaller charge transfer resistance. These results are consistent with the conductivity measured by four-point probe method in Table 1. For example, the conductivity of RGO film is 229.9 S m^{-1}. After hybridizing CPs with 30 wt%, the conductivities are slightly dropped to 197.8 S

m^{-1} (RGO/PANI30%) and 224.1 S m^{-1} (RGO/PPy30%). Further hybridizing CPs to 50 wt%, the conductivities are decreased to 147.4 S m^{-1} (RGO/PANI50%) and 182.1 S m^{-1} (RGO/PPy50%). In Figure 6c and 6d, 45° sloped portion can be observed in the low frequency region which is the Warburg resistance corresponding to the ion

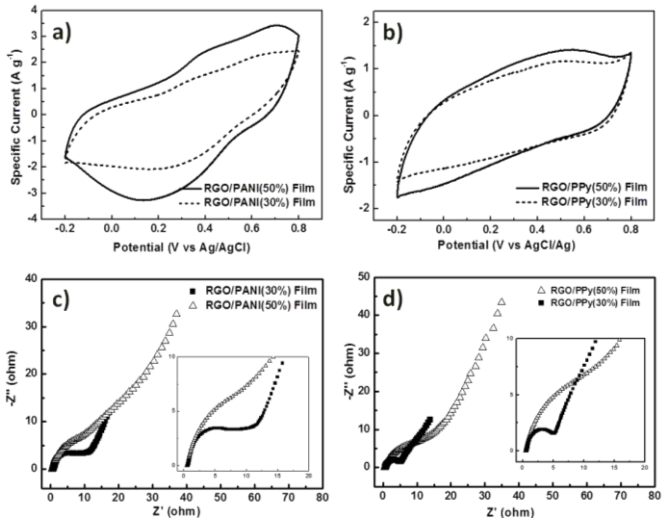

Figure 6: Cyclic voltammograms of RGO/PANI film electrodes (a), and RGO/PPy film electrodes (b); Nyquist plots of RGO/PANI film electrodes (c), and RGO/PPy film electrodes (d).

diffusion/transport in the electrolyte. A nearly vertical line usually can be seen at the very low frequency which is the characteristic feature an ideal capacitor.

The galvanostatic charge/discharge curves at the current density of 0.5 A g^{-1} are shown in Figure 7a. The discharging curves of RGO/PANI hybrid films exhibit two voltage stages, from 0.8 to 0.53 V and from 0.53 to -0.2 V, respectively. The relatively short discharging duration of the former stage is ascribed to the EDL capacitance. The much longer discharging duration for the latter one is associated with the combination of EDL capacitance and faradic capacitance of PANI nanofibres. The RGO/PPy hybrid films exhibit nearly triangular shape in the charge-discharge curve, indicating the pseudocapacitive contribution along with the double layer contribution. Gravimetric capacitances and volumetric capacitances of the hybrid film electrodes obtained in the present work are calculated from the galvanostatic charge/discharge curves. The gravimetric capacitance in Farads per gram was calculated from the galvanostatic discharge process according to the following equation: $C = I \times \Delta t/(\Delta V \times m)$, where I is the discharge current (A), Δt is the discharge time (s), ΔV is the voltage change (V) and m (g) is the total mass of the film electrode. The specific volumetric capacitance in Farads per cubic centimeter was calculated based on the gravimetric capacitance according the equation of $C_{vol} = C_{total} \times \rho$, where ρ (g cm^{-3}) is the density of films. These results are shown in Figure 7b and 7c, and selected capacitance values are summarized in Table 1. As listed in Table 1, the RGO/PANI(50%) and RGO/PANI(30%) film electrodes respectively gives rise to high gravimetric capacitances of 540 and 417 F g^{-1} at a current density of 0.2 A g^{-1}. Even at a current density of 2 A g^{-1}, high gravimetric capacitances of 369 and 298 F g^{-1} can be achieved with capacity retention of 68% and 71%, respectively. The volumetric capacitances of RGO/PANI(50%) and RGO/PANI(30%) film electrodes correspond to 616 and 525 F cm^{-3} at a current density of 0.2 A g^{-1}. The volumetric capacitance values of RGO/PANI hybrid films are compared favourably with those values reported for other graphene/PANI nanocomposites.[30, 34, 36-38] For example, CCG-PANI film electrode yielded a volumetric capacitance of 160 F cm^{-3} at a current density of 0.3 A g^{-1}.[28] The micro-supercapacitor fabricated based on PANI/Graphene electrode offered a volumetric capacitance of 436 F cm^{-3} at the scan rate of 10 mV s^{-1}.[20] RGO/PPy(50%) and RGO/PPy(30%) film electrodes yield gravimetric capacitances of 374 and 330 F g^{-1} at a current density of 0.2 A g^{-1} due to a more complete faradaic reaction at lower current density. The corresponding volumetric capacitances are calculated to be 355 and 340 F cm^{-3}, respectively. The hybrid film electrodes with high conducting polymer loading exhibit improved capacitance value compared

Table 1: The physical properties and selected electrochemical performances of RGO/CPs hybrid film electrodes.

Samples	Thickness (um)	Density (g cm^{-3})	Conductivity (S m^{-1})	Gravimetric capacitance (F g^{-1})			Volumetric capacitance (F cm^{-3})		
				0.2 A g^{-1}	2 A g^{-1}	5 A g^{-1}	0.2 A g^{-1}	2 A g^{-1}	5 A g^{-1}
RGO/PANI(50%) Film	8.7	1.14	147.4	540	369	237	616	421	270
RGO/PANI(30%) Film	7.9	1.26	197.8	417	298	256	525	376	323
RGO/PPy(50%) Film	10.5	0.95	182.1	374	218	170	355	207	162

RGO/PPy(30%) Film	9.7	1.03	224.1	330	214	168	340	220	173
RGO Film	7.5	1.33	229.9	85	63	52	113	84	69

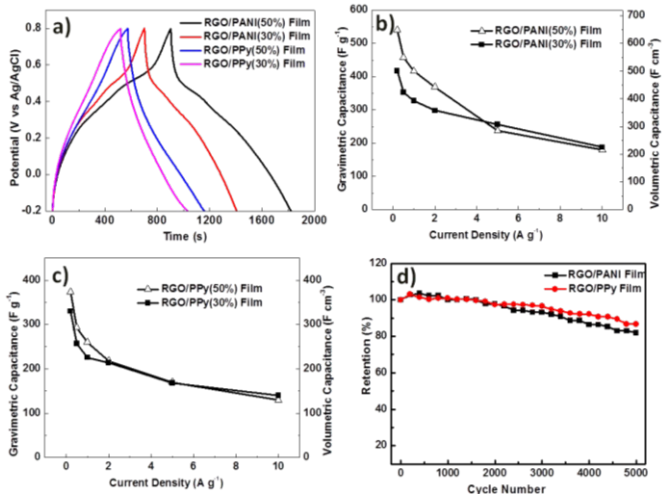

Figure 7: Galvanostatic charge-discharge curves of the hybrid film electrodes at the current density of 0.5 A g^{-1}(a); Gravimetric capacitance and volumetric capacitance of RGO/PANI film electrode (b) and RGO/PPy film electrode (c) at various current densities; Cycling performance of characteristic hybrid film electrodes at 2 A g^{-1} (d).

with their counterparts, resulting from a high contribution to pseudocapacitance from conducting polymers. However, comparable capacitance value is observed for the hybrid film electrodes at current densities higher than 5 A g^{-1}, which may well be due to the lack of response for faradaic reaction at high current density.

The cycling electrochemical stabilities of typical RGO/PANI(30%) and RGO/PPy(30%) electrodes were characterized by galvanostatic charge-discharge at a current density of 2 A g^{-1}, as shown in Figure 7d. 82% and 86% of the original capacitance were retained after 5000 cycles, correspondingly. It is well known that pure conducting polymers exhibit generally poor stability during cycling (as shown in Figure S4) due to the swelling and shrinkage of conducting polymers during doping-dedoping process. Graphene sheets and CNTs can provide a flexible, mechanically robust and electrically conductive network to accommodate the volume changes of conducting polymers, delivering charges/electrons efficiently to the current collectors, thus further improving the stability, which is highly favourable for prolonged charge–discharge cycle ability.

Conclusion

In summary, mechanically stable freestanding hybrid films were successfully fabricated by an extended filtration method via self-assembly of graphene and conducting polymers including polyaniline and polypyrrole. Owing to the synergistic effects of the constituent components in the hybrid composite structure and the merits of the well-preserved morphology and intrinsic properties of the components, the hybrid film electrodes exhibit high gravimetric capacitance, high volumetric capacitance, excellent rate capability and superior cycling stability. This new strategy provides a promising approach to bring graphene/conducting polymer hybrid materials to the fast and efficient energy storage in electrochemical devices.

Acknowledgements

The author thanks the financial support provided by MOE, Singapore Ministry of Education (Tier 2, MOE2012-T2-2-102). Author is also grateful to Eugene Shi Guang Choo, staff of ZEISS Advanced Imaging Centre (Singapore), who did the FIB cross-sectioning and imaging of the graphite composite materials.

References

1. P. Simon and Y. Gogotsi, *Nat. Mater.*, 2008, **7**, 845-854.
2. G. Wang, L. Zhang and J. Zhang, *Chem. Soc. Rev.*, 2012, **41**, 797-828.
3. P. Simon, Y. Gogotsi and B. Dunn, *Science*, 2014, **343**, 1210-1211.
4. L. L. Zhang, Y. Gu and X. S. Zhao, *J. Mater. Chem. A*, 2013, **1**, 9395-9408.
5. X. Wang, X. Lu, B. Liu, D. Chen, Y. Tong and G. Shen, *Adv. Mater.*, 2014, **26**, 4763-4782.
6. B. C. Kim, J.-Y. Hong, G. G. Wallace and H. S. Park, *Adv. Energy Mater.*, 2015, DOI: 10.1002/aenm.201500959.
7. W. Zeng, L. Shu, Q. Li, S. Chen, F. Wang and X.-M. Tao, *Adv. Mater.*, 2014, **26**, 5310-5336.
8. S. Stankovich, D. A. Dikin, G. H. B. Dommett, K. M. Kohlhaas, E. J. Zimney, E. A. Stach, R. D. Piner, S. T. Nguyen and R. S. Ruoff, *Nature*, 2006, **442**, 282-286.
9. A. K. Geim, *Science*, 2009, **324**, 1530-1534.
10. L. L. Zhang, R. Zhou and X. S. Zhao, *J. Mater. Chem.*, 2010, **20**, 5983.
11. X. Jiang, S. Setodoi, S. Fukumoto, I. Imae, K. Komaguchi, J. Yano, H. Mizota and Y. Harima, *Carbon*, 2014, **67**, 662-672.
12. C. Li, X. Zhang, K. Wang, H. Zhang, X. Sun and Y. Ma, *RSC Adv.*, 2014, **4**, 59603-59613.
13. C. Cheng and D. Li, *Adv. Mater.*, 2013, **25**, 13-30.
14. S. Park and R. S. Ruoff, *Nat. Nanotechnol.,* 2009, **4**, 217-224.
15. O. C. Compton and S. T. Nguyen, *Small*, 2010, **6**, 711-723.
16. X. Yang, J. Zhu, L. Qiu and D. Li, *Adv. Mater.*, 2011, **23**, 2833-2838.
17. M. Li, Z. Tang, M. Leng and J. Xue, *Adv. Funct. Mater.*, 2014, **24**, 7495-7502.
18. D. T. Pham, T. H. Lee, D. H. Luong, F. Yao, A. Ghosh, V. T. Le, T. H. Kim, B. Li, J. Chang and Y. H. Lee, *ACS Nano*, 2015, **9**, 2018-2027.
19. Y. Meng, K. Wang, Y. Zhang and Z. Wei, *Adv. Mater.*, 2013, **25**, 6985-6990.

20. Z.-S. Wu, K. Parvez, S. Li, S. Yang, Z. Liu, S. Liu, X. Feng and K. Müllen, *Adv. Mater.*, 2015, **27**, 4054.
21. X. Lu, W. Zhang, C. Wang, T.-C. Wen and Y. Wei, *Prog. Polym. Sci.*, 2011, **36**, 671-712.
22. L. Mao, K. Zhang, H. S. On Chan and J. Wu, *J. Mater. Chem.*, 2012, **22**, 80-85.
23. L. Mao, H. S. O. Chan and J. Wu, *RSC Adv.*, 2012, **2**, 10610-10617.
24. D. Li, M. B. Muller, S. Gilje, R. B. Kaner and G. G. Wallace, *Nat Nanotechnol.*, 2008, **3**, 101-105.
25. J. Huang and R. B. Kaner, *Angew. Chem. Int. Ed.*, 2004, **43**, 5817-5821.
26. X. Zhang, J. Zhang, Z. Liu and C. Robinson, *Chem. Commun.*, 2004, DOI: 10.1039/B405255B, 1852-1853.
27. X. Zhou, T. Wu, B. Hu, G. Yang and B. Han, *Chem. Commun.*, 2010, **46**, 3663-3665.
28. Q. Wu, Y. Xu, Z. Yao, A. Liu and G. Shi, *ACS Nano*, 2010, **4**, 1963-1970.
29. Y. Cheng, S. Lu, H. Zhang, C. V. Varanasi and J. Liu, *Nano Lett.*, 2012, **12**, 4206-4211.
30. Z. Tong, Y. Yang, J. Wang, J. Zhao, B.-L. Su and Y. Li, *J. Mater. Chem. A*, 2014, **2**, 4642-4651.
31. X. Chen, F. Meng, Z. Zhou, X. Tian, L. Shan, S. Zhu, X. Xu, M. Jiang, L. Wang, D. Hui, Y. Wang, J. Lu and J. Gou, *Nanoscale*, 2014, **6**, 8140-8148.
32. J. Liu, J. An, Y. Ma, M. Li and R. Ma, *J Electrochem. Soc.*, 2012, **159**, A828-A833.
33. Y. Yang, C. Wang, B. Yue, S. Gambhir, C. O. Too and G. G. Wallace, *Adv. Energy Mater.*, 2012, **2**, 266-272.
34. Q. Zhou, Y. Li, L. Huang, C. Li and G. Shi, *J.Mater.Chem. A*, 2014, **2**, 17489-17494.
35. C. Yu, P. Ma, X. Zhou, A. Wang, T. Qian, S. Wu and Q. Chen, *ACS Appl. Mater. Interfaces*, 2014, **6**, 17937-17943.
36. L. Mao, K. Zhang, H. S. On Chan and J. Wu, *J. Mater. Chem.*, 2012, **22**, 80-85.
37. K. Chi, Z. Zhang, J. Xi, Y. Huang, F. Xiao, S. Wang and Y. Liu, *ACS Appl. Mater. Interfaces*, 2014, **6**, 16312-16319.
38. Y. Meng, K. Wang, Y. Zhang and Z. Wei, *Adv. Mater.*, 2013, **25**, 6985-6990.

Bendable freestanding films composed of reduced graphene oxide and one dimensional conducting polymers exhibit superior capacitive performance in terms of gravimetric capacitance and volumetric capacitance.